Radiological Physics and Technology (2019) 12:268–276
https://doi.org/10.1007/s12194-019-00517-7

Dosimetric assessment of a single-energy metal artifact reduction algorithm for computed tomography images in radiation therapy

Hiroo Murazaki[1] · Junichi Fukunaga[1] · Taka-aki Hirose[1] · Naomi Funatsu[1] · Ryoji Matsumoto[1] · Kyohei Hidaka[1] · Shuji Nagamine[1] · Daiki Nakanishi[1] · Toyoyuki Kato[1]

Received: 2 March 2019 / Revised: 21 May 2019 / Accepted: 22 May 2019 / Published online: 28 May 2019

Abstract
This study aimed to evaluate the performance of a single-energy metal artifact reduction (SEMAR) algorithm for radiation therapy treatment using phantom cases with metal inserts, assess improvements in computed tomography (CT) number accuracy, and investigate its effects on treatment planning dosimetry. A standard electron density phantom was scanned with and without metal inserts. The numbers of tissue-equivalent materials on both uncorrected and SEMAR-corrected CT images were compared. Treatment planning accuracy was evaluated by comparing dose distributions computed using true density images (without metal inserts), uncorrected images (with metal inserts), and SEMAR-corrected images (with metal inserts) using three-dimensional gamma analysis. The numbers of the true density and uncorrected and SEMAR-corrected CT images in a muscle plug with unilateral inserts were 25.9 HU, −281.8 HU, and 26.1 HU, respectively. A similar tendency was obtained for other tissue-equivalent materials, and the numbers on CT images were improved with the SEMAR algorithm. In cases involving 1 portal irradiation, 10-MV X-ray, and the Acuros XB algorithm, the pass ratio between the true density and uncorrected images was 89.89%, while that between the true density and SEMAR-corrected images was 95.03%. Improvements in dose distribution were evident using the SEMAR algorithm. Similar trends were found for different irradiation methods and dose calculation algorithms. The SEMAR algorithm can significantly reduce metal artifacts on CT images used for radiation treatment planning. This aspect influenced dosimetry in the region of the artifact and dose distribution was significantly improved with use of the SEMAR-corrected images.

Keywords Metal artifact reduction · Single-energy metal artifact reduction · Radiation treatment planning · Dose distribution

1 Introduction

In radiotherapy planning, computed tomography (CT) images are widely used to delineate gross tumor volumes and at-risk organs, which enables the calculation of the dose distribution to each structure [1]. It is important to accurately reproduce the relationship between electron density (ED) of the tissue and the CT value to ensure the accuracy of CT-based radiotherapy planning. One factor affecting treatment plan accuracy is the presence of metal artifacts. For example, metallic implants, especially hip prostheses, can produce severe CT image artifacts. These artifacts not only jeopardize the radiation oncologist's confidence in tumor and organ delineation, but also severely affect CT number accuracy. When developing a treatment plan using CT images distorted and obscured by metal artifacts, clinicians must rely on educated guesses when contouring both targets and critical structures based on their clinical experience. In practice, it can be necessary for clinicians to manually override artifact regions to an artificial ED to partially account for tissue heterogeneity. Additionally, in methods that use a manual override of the area of air using the ED of water, if the override is erroneous, the dose calculation error increases. Many metal artifact reduction techniques for CT images have been described in the literature, such as those based on image reconstruction processing and dual-energy imaging [2–8]. A method for metal artifact reduction processing was also developed. Additionally, the SEMAR

✉ Hiroo Murazaki
murasaki@r-tec.med.kyushu-u.ac.jp

[1] Division of Radiology, Department of Medical Technology, Kyushu University Hospital, 3-1-1 Maidashi, Fukuoka 812-8582, Japan

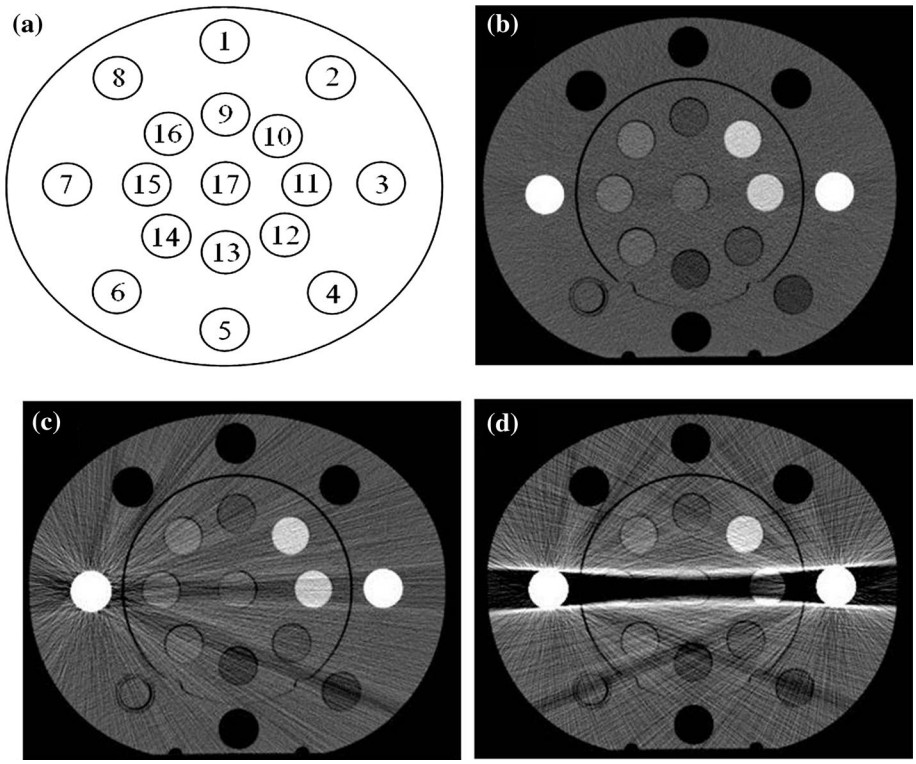

Fig. 1 **a** Distribution of the insert materials presented in Table 1. Computed tomography image of the phantom (Computerized Imaging Reference Systems, Inc., Norfolk, VA, USA) acquired without a metal insert (**b**), with a unilateral metal insert (**c**), and with bilateral metal inserts (**d**)

algorithm (Canon Medical Systems Corporation, Otawara, Tochigi Prefecture, Japan) is a new solution that has been proposed for clinical implementation [9–12]. The SEMAR algorithm can extract metal from the original image using a simple fixed- or automatic-threshold approach to create a sinogram of the metal only. The original sinogram is subtracted from the metal-only sinogram and linear interpolation is performed to create a metal-free sinogram. Furthermore, the metal object is eliminated with the intermediate data and, ultimately, a final image is obtained by blending of the reconstructed image with the metal image [13, 14]. Studies in the diagnostic field involving the SEMAR algorithm reported image quality improvements based on visual inspection [9–12]. It is intuitive that contour extraction accuracy can be improved by reducing metal artifacts. However, because dosimetric accuracy directly depends on the CT value, improvements in dose calculation accuracy are expected when the CT value of the artifact part is improved. In addition, the influences of SEMAR on dose distribution were studied in carbon-ion therapy [15] or brachytherapy [16].

However, the dose calculation algorithms of these approaches differ from that of external beam radiation therapy using X-rays. Furthermore, unlike gamma and alpha rays, X-rays used for external beam radiation therapy differ in energy and properties. Therefore, the present study aimed to evaluate the performance of the SEMAR algorithm in external beam radiation therapy treatment with X-rays on phantom cases with large metal implants, assess improvements in CT number accuracy, and investigate its effects on dose calculation accuracy.

2 Materials and methods

2.1 CT scanning

A standard ED phantom (Model 062A; Computerized Imaging Reference Systems, Inc., Norfolk, VA, USA) was aligned at the center of the field of view and scanned with/without metal inserts (Ti-6Al-4V; Tokyo Implant, Saitama, Japan). The ED phantom is made from water-equivalent materials (physical density, 1.02 g/cm^3) with dimensions of 330 mm (width) × 270 mm (height) × 250 mm (depth). The diameter of each plug is approximately 30 mm. Either tissue-equivalent plugs or one or two implants were inserted into the left and right cavities of the ED phantom to simulate none, unilateral, and bilateral hip implants (Fig. 1).

The physical density value of each plug was 0.20–1.53 g/cm^3. Several plugs with physical densities (range 0.96–1.16 g/cm^3) similar to soft tissue were centered between the metal implants to simulate critical structures within the human body.

All CT scans were performed using an 80-detector-row CT scanner (Aquilion PRIME; Canon Medical Systems, Otawara, Japan). The scan parameters were as follows:

scan mode, helical; tube voltage, 120 kV; detector collimation 0.5 × 80 mm; slice thickness 2.0 mm; helical pitch 75; gantry rotation time 0.5 s; reconstruction field of view 500 mm; matrix 512 × 512; abdomen standard reconstruction kernel (FC13); and CTDIvol 20.3 mGy. The tube current was automatically adjusted with the image noise level (standard deviation of the CT number) of the automatic exposure control technique. The image noise level was set at 10 HU. First, a metal artifact-free image (without a metal image) was acquired by placing bone-equivalent plugs with a physical density of 1.53 g/cm^3 in locations 3 and 7 of the ED phantom for use as the reference image. Second, to simulate a unilateral implant, the bone-equivalent plug in location 7 was replaced with a metal insert. Finally, the bone-equivalent implants in locations 3 and 7 were replaced with metal implants to simulate bilateral implants. CT scans were repeated three times. CT imaging of the phantom, with unilateral or bilateral implants, was performed using the SEMAR algorithm. The five data sets (i.e., without metal image, with a unilateral metal image, with a unilateral metal image corrected with SEMAR, with bilateral metal images, and with bilateral metal images corrected with SEMAR) were analyzed according to CT number and dose calculation accuracy.

2.2 CT number accuracy

For each image set, three slices of the center region of the ED phantom were used to measure CT number. The CT number for each density plug was measured on all scans using a 20-pixel-diameter region of interest (ROI), and calculated as the mean value of three contiguous slice images. Image noise (σ) was calculated as the root mean square value of the standard deviation of the CT number in these three images. CT number and noise differences were calculated using the following equations:

$$\text{CT\# difference} = \left|\text{CT\#} - \text{CT\#}_{\text{standard}}\right|,$$

$$\text{Noise difference} = \left|\sigma - \sigma_{\text{standard}}\right|,$$

where CT# is the mean CT number obtained for ED phantoms with a metal insert using SEMAR-corrected and -uncorrected images, $\text{CT\#}_{\text{standard}}$ is the mean CT number obtained for ED phantoms without metal inserts, σ is the mean standard deviation obtained for ED phantoms with metal insert using SEMAR-corrected and -uncorrected images, and σ_{standard} is the mean standard deviation obtained for ED phantoms without metal inserts.

2.3 Dose calculation accuracy

A quantitative dosimetry evaluation was conducted of each of the five image sets using single-field irradiation, opposite portal irradiation, four-field irradiation, and volumetric modulated arc therapy (VMAT) at 10 MV. All dose calculations were performed using the Eclipse treatment planning system (Varian Medical Systems version 13.6.30, Palo Alto, CA, USA) with the Acuros XB algorithm (AXB; Varian Medical Systems, Palo Alto, CA, USA) and the anisotropic analytical algorithm (AAA). The following parameters were used for each irradiation: photon energy, 10 MV; prescribed radiation dose, 2 Gy; dose calculation algorithm, AXB, AAA; calculation grid 1.5 mm; beam angle, one field irradiation 0°; opposing portal irradiation 0° and 180°; four-field irradiation 45°, 135°, 225°, 315°, VMAT; unilateral 0°–240°, 300°–360°; and bilateral 0°–60°, 120°–240°, 300°–360°. In the case of VMAT, the beam angles were chosen to avoid the metal along their path in the phantom and the unilateral and bilateral used single and double arcs, respectively. All plans were created using the original CT set without the metal insert, after which they were recalculated using the same geometry and monitor unit number for SEMAR-uncorrected or -corrected images with the metal insert. No density overrides were made to the artifact regions on the metal-contaminated images for the dose calculations. The dose distributions calculated on the SEMAR-corrected and -uncorrected images were compared with the dose distribution calculated on an image of the phantom with no metal implant. A three-dimensional gamma analysis ($\gamma < 1$, 1%/0 mm) was performed using a DD system (version 12-3; R-TECH Inc., Tokyo, Japan), while the pass rate was compared using the SEMAR-corrected and -uncorrected images. Inter-calculation differences were tested using the Wilcoxon signed rank test for paired data at a significance level of 0.05.

3 Results

3.1 CT number accuracy

Images representative of the phantom data for SEMAR-corrected and -uncorrected images are presented in Fig. 2. For the single-insert scenario, the streak artifact was reduced using the SEMAR algorithm. However, no improvement in CT number was evident (Figs. 2a, 3). For the double-insert scenario, the streak artifact was dramatically reduced using the SEMAR algorithm, while the CT number accuracy was dramatically improved in plugs #11, #15, and #17 (Figs. 2b, 4). As shown in Fig. 4, the CT number difference for the muscle-equivalent plug #17 in the uncorrected image is 307.7 HU compared with a CT number difference of 0.3 HU for the SEMAR-corrected image. Similarly, for the bone-equivalent plug #11 and liver-equivalent plug #15, the CT number differences were improved from 281.5 to 17.0 HU and from 278.4 to 1.7 HU, respectively. The noise difference

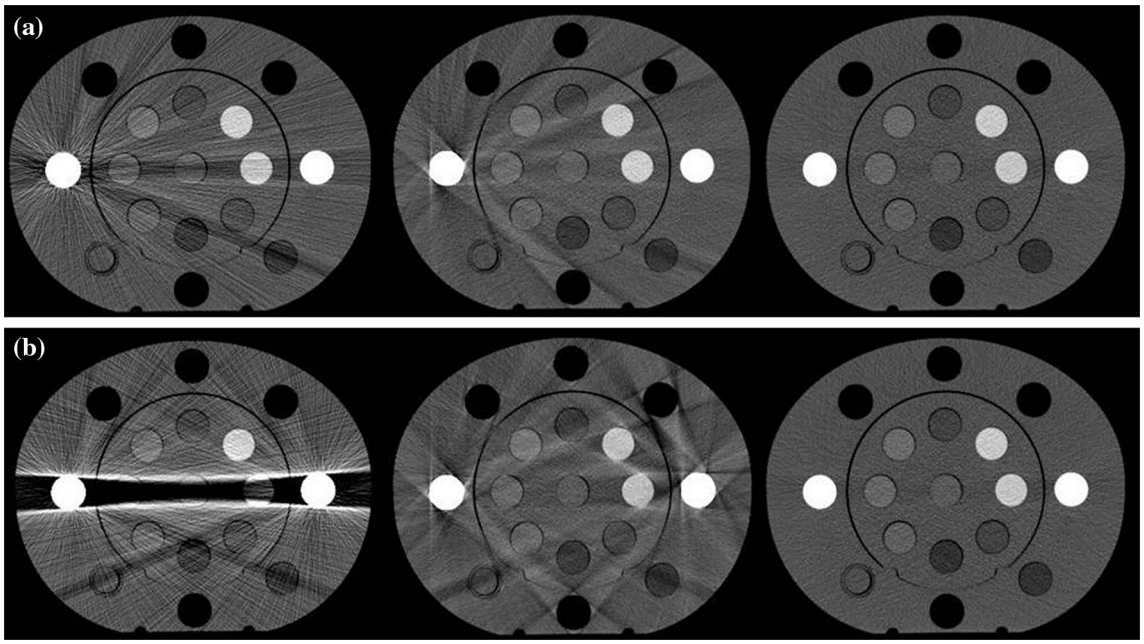

Fig. 2 The left panels depict the original image with metal artifacts using a unilateral metal insert (**a**) and bilateral metal inserts (**b**). The middle panels depict single-energy metal artifact reduction (SEMAR)—corrected images. The right panels are the original images without the metal inserts

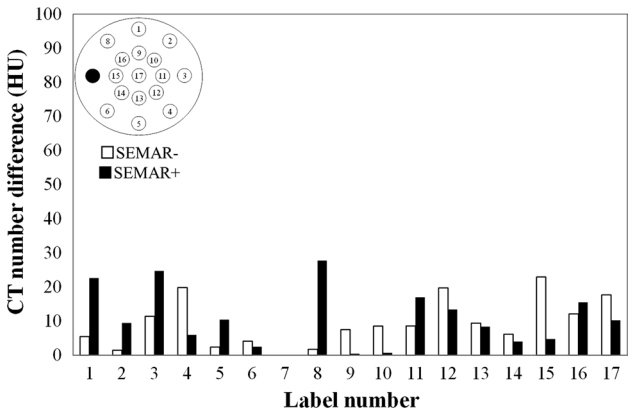

Fig. 3 Computed tomography (CT) number difference obtained by subtracting the mean CT number obtained without a metal insert from the mean CT number with a unilateral metal insert obtained using single-energy metal artifact reduction (SEMAR)—corrected and -uncorrected images

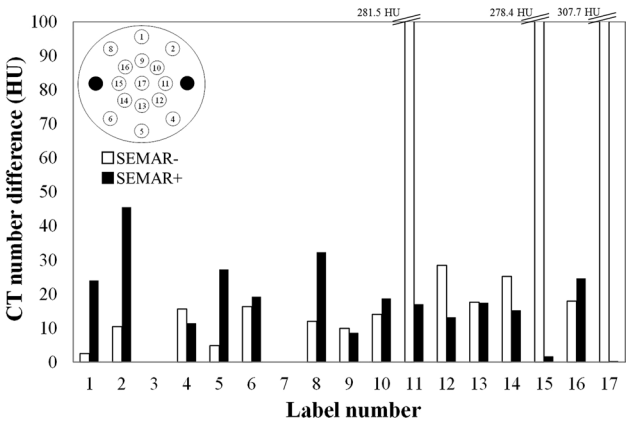

Fig. 4 Computed tomography (CT) number difference obtained by subtracting the mean CT number obtained without a metal insert from the mean CT number with bilateral metal inserts obtained using single-energy metal artifact reduction (SEMAR)—corrected and -uncorrected images

was improved in the SEMAR-corrected images compared with the SEMAR-uncorrected images for the unilateral and bilateral implants (Figs. 5, 6).

3.2 Dose calculation accuracy

Figures 7 and 8 depict the gamma analysis map using SEMAR-uncorrected and -corrected data on single-field irradiation and VMAT. The red dots indicate that the dose difference did not meet the necessary criteria (1%, 0 mm). For both single-field irradiation and VMAT, the red dots decreased with use of the SEMAR algorithm. The decrease in the red dots was larger in the bilateral implant than in the unilateral implant. The pass rates with the SEMAR-corrected and -uncorrected images for each irradiation method and dose calculation algorithm are shown in Table 2. In many cases, using the SEMAR algorithm significantly improved the pass rates. However, when the phantom was

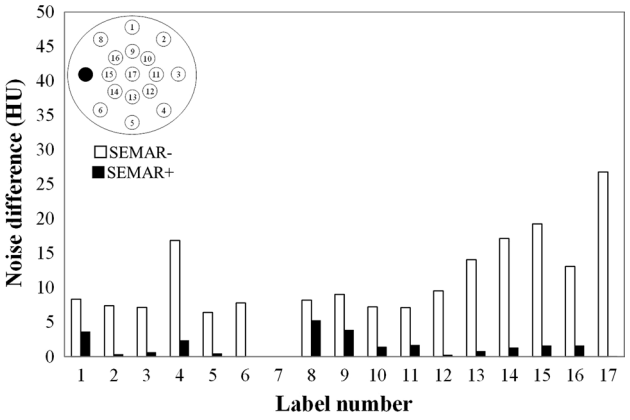

Fig. 5 Noise difference obtained by subtracting the mean computed tomography number obtained without a metal insert from the mean standard deviation with a unilateral metal insert obtained using single-energy metal artifact reduction (SEMAR)—corrected and -uncorrected images

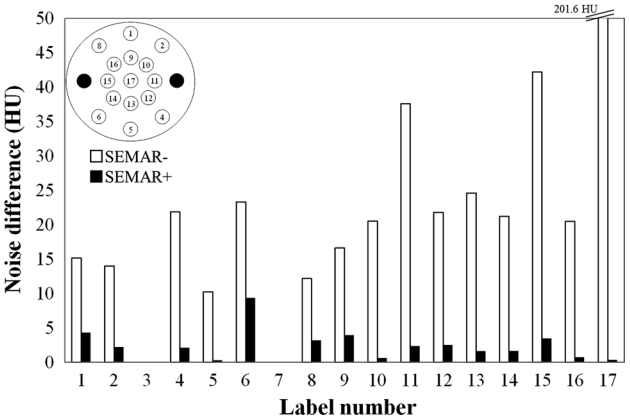

Fig. 6 Noise difference obtained by subtracting the mean computed tomography number obtained without a metal insert from the mean standard deviation with bilateral metal inserts obtained using single-energy metal artifact reduction (SEMAR)—corrected and -uncorrected images

implanted unilaterally, no improvements were observed for any irradiation method and no significant differences were observed when the AAA algorithm was used.

4 Discussion

The present study evaluated the utility of the SEMAR algorithm for radiation therapy planning by performing a physical evaluation using a standard ED phantom. To evaluate streak artifacts caused by metal implant(s), CT number accuracy was evaluated. The results indicated that SEMAR-corrected images accurately recovered their CT numbers for phantom data (Figs. 3, 4). Furthermore, image noise was also improved (Figs. 5, 6), as was image uniformity (Fig. 3). On the other hand, in the case of plugs whose CT values significantly differed from the baseline CT value of the ED phantom, such as the lung (inhale and exhale) or bone (300 and 800 mg/cm^3), the CT value deteriorated when the SEMAR algorithm was used. Because a partial volume effect occurs around the metal region in which the CT value has decreased, segmentation of metal parts in the iteratively reconstructed original image becomes insufficient and affects subsequent processing. Additionally, the path through the boundary between the base and the plug with a large difference in CT value where the number of photons reaching the detector is low and a point where it can be extracted as metal and a point where it cannot be extracted are mixed. Therefore, the CT value is unreliable, affecting the processing of metal extraction and leaving artifacts. It is possible that these effects combine to cause artifacts and affect the CT values.

4.1 Dosimetric comparison

Each dose calculation algorithm was evaluated using a gamma analysis to assess dose calculation accuracy. In our study, a dose difference ≥ 1% was observed in the metal artifact area and the build-up region. The dose distribution using SEMAR-corrected images was significantly improved compared with that of the SEMAR-uncorrected images. Axente et al. [17] reported that a gamma analysis of the region most affected by the metal artifacts captured the relative improvement in local dosimetry when the iterative metal artifact reduction-corrected image was used for the calculation. This finding is consistent with our results. However, when the AAA was used as the dose calculation algorithm in unilaterally implanted phantoms, there were no significant differences among the opposing portal irradiation, four-field irradiation, and VMAT. It is known that the dose calculation accuracy obtained using the AXB is similar to that obtained using the Monte Carlo (MC) simulation or the measured does compared to that obtained using the AAA [18–23]. In a study by Lloyd et al. [24], stainless steel was placed in the water-equivalent phantom and the dose distribution was calculated using AAA, AXB, and MC simulation. The AXB and MC simulation findings were in good agreement with regard to the percent depth dose and the off-axis ratio at the periphery of the high-density material. High-density objects introduce streak artifacts in CT images, which in turn affect tissue HU values and the generation of a dose distribution that accurately reflects patient geometry. In this study, because the AAA has low-dose calculation accuracy, improvements in metal artifacts using the SEMAR algorithm may not be reflected in the dose distribution calculation. On the other hand, because the AXB has high-dose calculation

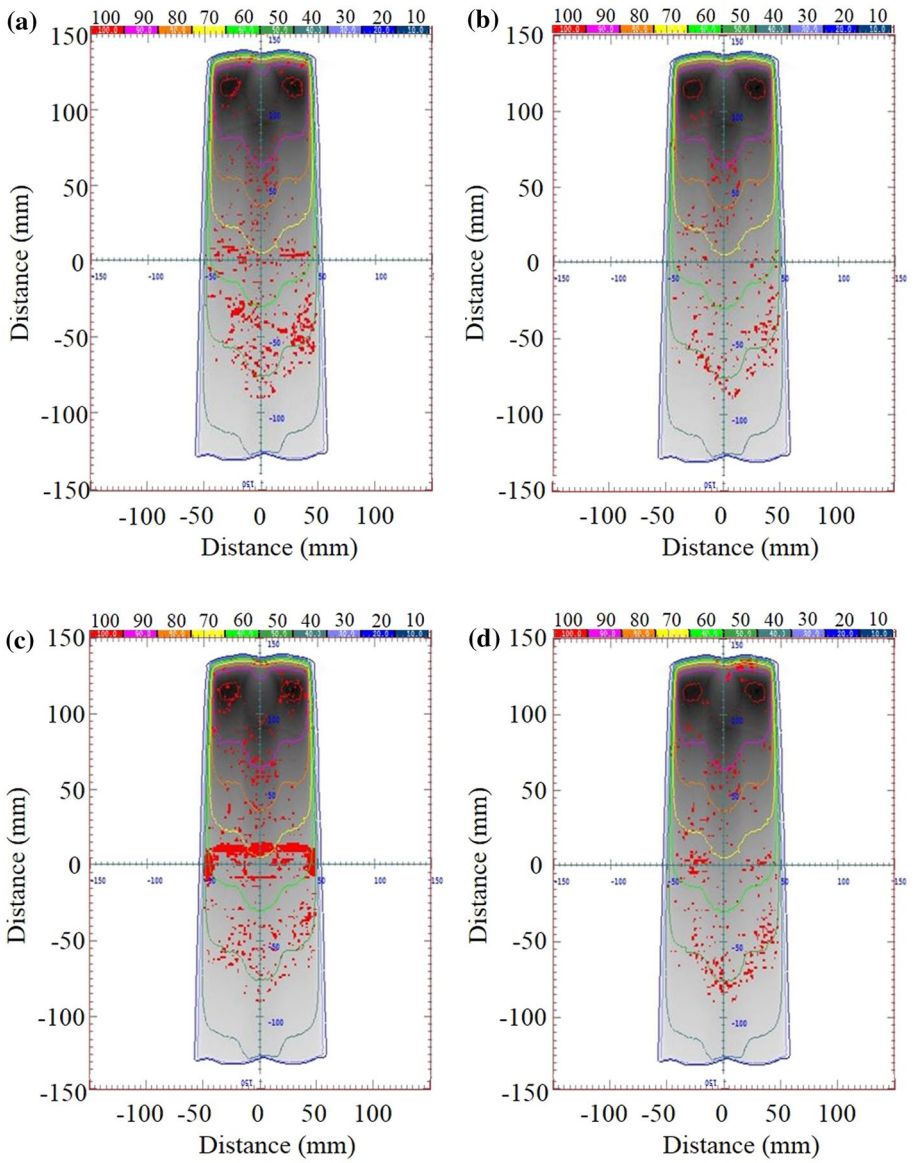

Fig. 7 Dose difference maps using single-energy metal artifact reduction (SEMAR)–corrected and -uncorrected images with the Acuros XB algorithm (Varian Medical Systems, Palo Alto, CA, USA) and single-field irradiation. The upper panels depict a unilateral metal insert using a SEMAR-uncorrected image (**a**) and a SEMAR-corrected image (**b**). The lower panels depict a bilateral metal insert using a SEMAR-uncorrected image (**c**) and a SEMAR-corrected image (**d**)

accuracy, improvements in metal artifacts using the SEMAR algorithm are reflected in the dose distribution calculation.

5 Limitations

In the dosimetric comparison, an image with no artifacts was used as the gold standard. We did not compare our results to those obtained using MC simulation or the measured dose. In this study, the CT scan is assumed to be a clinical condition and the scan parameters are not changed. Improvements in the artifacts are expected by imaging using a high tube voltage scan technique and changed slice thickness and radiation dose. To compare the dose distribution SEMAR-uncorrected and -corrected images, no density overrides were made to the artifact regions on the metal-contaminated images for dose calculations. Further studies are needed on the usefulness of SEMAR compared to methods that manually override the area of air using the ED of water.

6 Conclusion

The results of the present study indicate that the SEMAR algorithm can significantly reduce metal artifacts on CT images used for radiation treatment planning, which consequently produces significantly more accurate CT numbers in the SEMAR-corrected images. This aspect influenced dosimetry in the region of the artifact, and the use of

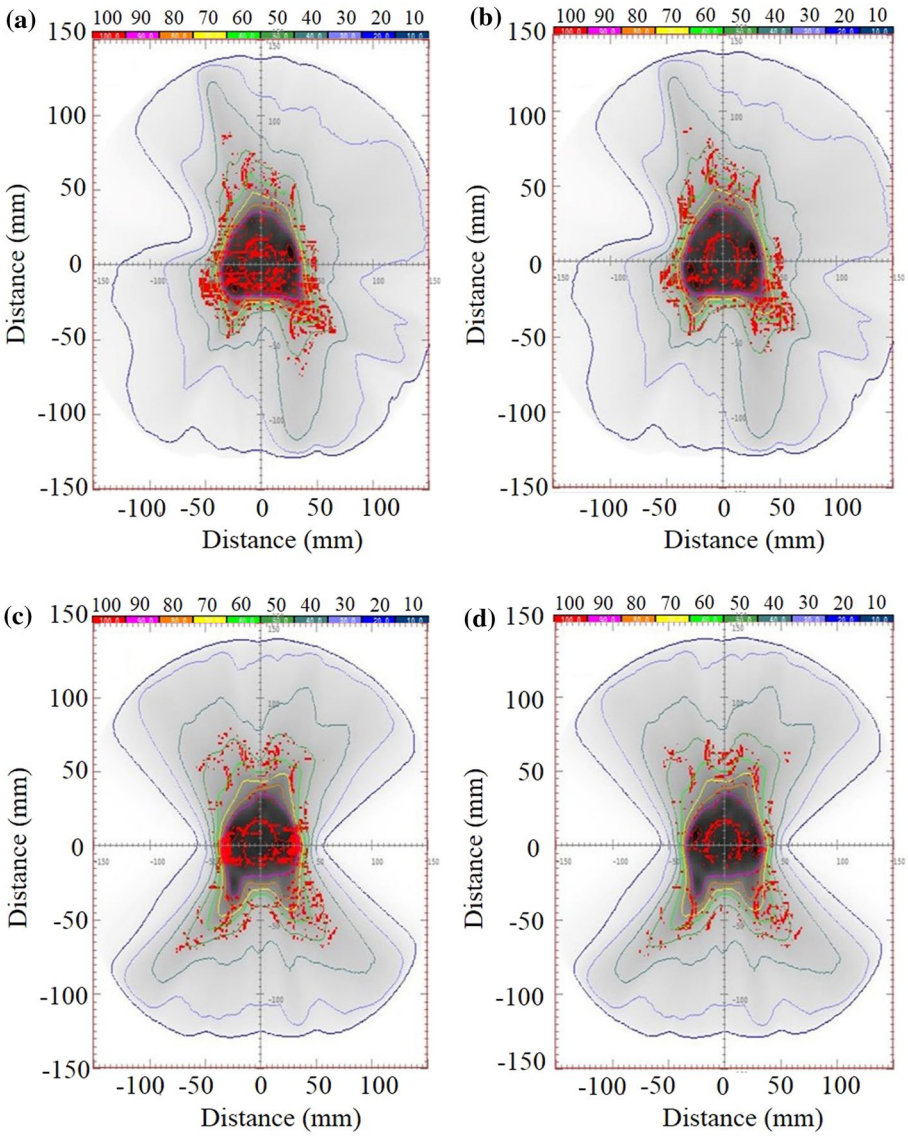

Fig. 8 Dose difference maps using single-energy metal artifact reduction (SEMAR)-corrected and -uncorrected images using the Acuros XB algorithm (Varian Medical Systems, Palo Alto, CA, USA) and volumetric modulated arc therapy. The upper panels depict a unilateral metal insert using a SEMAR-uncorrected image (**a**) and a SEMAR-corrected image (**b**). The lower panels depict bilateral metal inserts using a SEMAR-uncorrected image (**c**) and a SEMAR-corrected image (**d**)

Table 1 Tissue equivalents of materials used as CIRS phantom inserts

Label No	Insert label	Physical density (g/cm^3)	Electron density ($\times 10^{23}$ electrons/g)	Mean Huref values (120 kVp)
1 and 8	Lung (inhale)	0.20	0.634	−821.0, −818.5
2 and 5	Lung (exhale)	0.50	1.632	−492.4, −4.88.5
3 and 7	Bone (800 mg/cm^3)	1.53	4.862	904.4, 909.1
4 and 13	Adipose	0.96	3.171	−51.1, −53.7
6	Removable vial	1.00	3.340	4.7
9 and 12	Breast 50/50	0.99	3.261	−23.2, −20.1
10 and 11	Bone (200 mg/cm^3)	1.16	3.73	242.6, 234.4
14 and 17	Muscle	1.06	3.483	34.3, 25.9
15 and 16	Liver	1.07	3.516	49.9, 57.5

The label indices correspond to the labels seen in Fig. 1

Table 2 Pass ratio for each beam configuration

	Single-field irradiation			Opposing portal irradiation			Four-field irradiation			VMAT		
	SEMAR− (%)	SEMAR+ (%)	*p* value	SEMAR− (%)	SEMAR+ (%)	*p* value	SEMAR− (%)	SEMAR+ (%)	*p* value	SEMAR− (%)	SEMAR+ (%)	*p* value
AAA												
Unilateral	98.72	97.94	0.039	99.03	98.83	0.426	99.83	99.75	0.188	100	100	1.000
Bilateral	94.56	97.07	0.004	96.64	97.33	0.039	98.90	99.15	0.008	89.52	100	0.004
Acuros												
Unilateral	91.13	93.91	0.004	92.12	93.59	0.004	94.47	95.85	0.004	88.50	92.44	0.004
Bilateral	86.90	92.20	0.004	89.76	92.09	0.004	92.32	92.96	0.074	85.88	92.27	0.004

Differences in comparisons between calculations was tested using the Wilcoxon signed rant test for paired data with a significance level of 0.05

SEMAR-corrected images significantly improved the dose distribution.

Compliance with ethical standards

Conflict of interest The authors declare no conflicts of interest.

Ethical approval This article contains no studies with human participants or animals.

Informed consent Informed consent for this study was not required because it involved no research involving human participants.

References

1. Mutic S, Palta JR, Butker EK, Das IJ, Huq MS, Loo LND, et al. Quality assurance for computed-tomography simulators and the computedtomography-simulation process: report of the AAPM radiation therapy committee task group no. 66. Med Phys. 2003;30:2762–92.
2. Hoyoshi K, Satou T, Okada A. Effect of hybrid iterative reconstruction on CT image quality using metal artifact reduction. Nihon Hoshasen Gijutsu Gakkai Zasshi. 2018;74:797–804.
3. Katsura M, Sato J, Akahane M, Tajima T, Furuta T, Mori H, et al. Single-energy metal artifact reduction technique for reducing metallic coil artifacts on post-interventional cerebral CT and CT angiography. Neuroradiology. 2018;60:1141–50.
4. Niehues SM, Vahldiek JL, Troltzsch D, Hamm B, Shnayien S. Impact of single-energy metal artifact reduction on CT image quality in patients with dental hardware. Comput Biol Med. 2018;103:161–6.
5. Bal M, Spies L. Metal artifact reduction in CT using tissue-class modeling and adaptive prefiltering. Med Phys. 2006;33:2852–9.
6. Kalender WA, Hebel R, Ebersberger J. Reduction of CT artifacts caused by metallic implants. Radiology. 1987;164:576–7.
7. Watzke O, Kalender WA. A pragmatic approach to metal artifact reduction in CT: merging of metal artifact reduced images. Eur Radiol. 2004;14:849–56.
8. Yazdia M, Gingras L, Beaulieu L. An adaptive approach to metal artifact reduction in helical computed tomography for radiation therapy treatment planning: experimental and clinical studies. Int J Radiat Oncol. 2005;62:1224–31.
9. Ragusi M, van der Meer RW, Joemai RMS, van Schaik J, van Rijswijk CSP. Evaluation of CT angiography image quality acquired with single-energy metal artifact reduction (SEMAR) algorithm in patients after complex endovascular aortic repair. Cardiovasc Intervent Radiol. 2018;41:323–9.
10. Ragusi MAAD, der Meer RW, Joemai RMS, van Schaik J, van Rijswijk CSP. Evaluation of CT angiography image quality acquired with single-energy metal artifact reduction (SEMAR) algorithm in patients after complex endovascular aortic repair. Cardiovasc Inter Rad. 2018;41:323–9.
11. Teixeira PAG, Meyer JB, Baumann C, Raymond A, Sirveaux F, Coudane H, et al. Total hip prosthesis CT with single-energy projection-based metallic artifact reduction: impact on the visualization of specific periprosthetic soft tissue structures. Skelet Radiol. 2014;43:1237–46.
12. Funama Y, Taguchi K, Utsunomiya D, Oda S, Hirata K, Yuki H, et al. A newly-developed metal artifact reduction algorithm improves the visibility of oral cavity lesions on 320-MDCT volume scans. Phys Med. 2015;31:66–71.

13. Chang YB, Xu D, Zamyatin AA. Metal artifact reduction algorithm for single energy and dual energy CT scans. In: IEEE Nuclear science conference record. 2012;3426–29.
14. Kidoh M, Utsunomiya D, Ikeda O, Tamura Y, Oda S, Funama Y, et al. Reduction of metallic coil artefacts in computed tomography body imaging: effects of a new single-energy metal artefact reduction algorithm. Eur Radiol. 2016;26:1378–86.
15. Miki K, Mori S, Hasegawa A, Naganawa K, Koto M. Single-energy metal artefact reduction with CT for carbon-ion radiation therapy treatment planning. Br J Radiol. 2016;89:20150988.
16. Shiraishi Y, Yamada Y, Tanaka T, Eriguchi T, Nishimura S, Yoshida K, et al. Single-energy metal artifact reduction in post-implant computed tomography for I-125 prostate brachytherapy: impact on seed identification. Brachytherapy. 2016;15:768–73.
17. Axente M, Paidi A, Von Eyben R, Zeng C, Bani-Hashemi A, Krauss A, et al. Clinical evaluation of the iterative metal artifact reduction algorithm for CT simulation in radiotherapy. Med Phys. 2015;42:1170–83.
18. Han T, Mourtada F, Kisling K, Mikell J, Followill D, Howell R. Experimental validation of deterministic Acuros XB algorithm for IMRT and VMAT dose calculations with the Radiological Physics Center's head and neck phantom. Med Phys. 2012;39:2193–202.
19. Han T, Mikell J, Salehpour M, Mourtada F. Dosimetric comparison of acuros XB Deterministic radiation transport method with Monte Carlo and model-based convolution methods in heterogeneous media. Med Phys. 2011;38:2651–64.
20. Padmanaban S, Warren S, Walsh A, Partridge M, Hawkins MA. Comparison of Acuros (AXB) and Anisotropic Analytical Algorithm (AAA) for dose calculation in treatment of oesophageal cancer: effects on modelling tumour control probability. Radiat Oncol. 2014;9:286.
21. Kroon PS, Hol S, Essers M. Dosimetric accuracy and clinical quality of Acuros XB and AAA dose calculation algorithm for stereotactic and conventional lung volumetric modulated arc therapy plans. Radiat Oncol. 2013;8:149.
22. Ong CCH, Ang KW, Soh RCX, Tin KM, Yap JHH, Lee JCL, et al. Dosimetric comparison of peripheral NSCLC SBRT using Acuros XB and AAA calculation algorithms. Med Dosim. 2017;42:216–22.
23. Nagata K, Pethel TD. A comparison of two dose calculation algorithms-anisotropic analytical algorithm and Acuros XB-for radiation therapy planning of canine intranasal tumors. Vet Radiol Ultrasoun. 2017;58:479–85.
24. Lloyd SAM, Ansbacher W. Evaluation of an analytic linear Boltzmann transport equation solver for high-density inhomogeneities. Med Phys. 2013;40:011707. https://doi.org/10.1118/1.4769419.